Available online at www.sciencedirect.com
ScienceDirect
Spectrochimica Acta Part A 69 (2008) 1020–1026
SPECTROCHIMICA ACTA PART A
www.elsevier.com/locate/saa

Synthesis, thermal, spectroscopic and magnetic studies of the $Mn(SeO_3)\cdot 2H_2O$ and $Fe_2(SeO_3)_3\cdot 3H_2O$ selenites

Aitor Larrañaga [a], José L. Mesa [b,*], José L. Pizarro [a], Luis Lezama [b], María I. Arriortua [a], Teófilo Rojo [b]

[a] *Departamento de Mineralogía y Petrología, Facultad de Ciencia y Tecnología, Apdo. 644, 48080 Bilbao, Spain*
[b] *Departamento de Química Inorgánica, Facultad de Ciencia y Tecnología, Apdo. 644, 48080 Bilbao, Spain*

Received 12 December 2006; accepted 2 June 2007

Abstract

$Mn(SeO_3)\cdot 2H_2O$ (**1**) and $Fe_2(SeO_3)_3\cdot 3H_2O$ (**2**) have been synthesized by slow evaporation from an aqueous solution in the case of (**1**) and using mild hydrothermal conditions for (**2**). The crystal structures of both phases have been refined by the Rietveld method. The compounds crystallize in different spatial groups, the $P2_1/n$ monoclinic one with parameters $a = 6.649(1)$ Å, $b = 6.542(1)$ Å, $c = 10.890(1)$ Å and $\beta = 103.85(1)^\circ$ being $Z = 4$ for (**1**) and the $R3c$ trigonal space group with parameters $a = 9.361(1)$ Å, $c = 20.276(1)$ Å and $Z = 6$ for (**2**). The crystal structure of compound (**1**) consists of a three-dimensional framework formed by MnO_6 octahedra and $(SeO_3)^{2-}$ oxoanions with trigonal pyramidal geometry, which gives rise to Mn_2O_{10} dimers of edge-sharing octahedra. The crystal structure of phase (**2**) can be described as a three-dimensional framework formed by MnO_6 octahedra and $(SeO_3)^{2-}$ oxoanions with trigonal pyramidal geometry. In this phase the octahedral entities are linked along the three crystallographic axes through the selenite anions. Diffuse reflectance spectrum and luminescent measurements for (**1**) indicate the existence of Mn^{2+} cations in a slightly distorted octahedral environment. Diffuse reflectance spectrum and Mössbauer spectroscopy, in the paramagnetic region, for (**2**) show the existence of Fe^{3+} cations in slightly distorted octahedral symmetry. ESR spectra of both compounds are isotropic with a *g*-value of 1.99(1) and 2.00(1), respectively. Magnetic measurements of both phases indicate an antiferromagnetic behavior. For phase (**2**), both, the ESR and magnetic measurements suggest a spin change from Fe^{3+} ($S = 5/2$) to Fe^{2+} ($S = 2$) at low temperatures.

Keywords: UV–vis; Thermal behavior; Mössbauer; ESR; Magnetism

1. Introduction

An important area in material science is the design of compounds with a condensed framework, which can give rise to original physical properties due to the great number of different cation arrangements that they can exhibit [1]. It is noteworthy that the ubiquitous presence of a stereochemically active lone-pair of electrons on the Se(IV) centers can play an important role in the crystalline architecture of these families of compounds [2]. The entire structure is affected by the requirement for empty space to accommodate the selenium lone-pair electron. Thus, it can be predicted that the combination of the inherently asymmetric $(SeO_3)^{2-}$ group with various transition metals will result in a rich structural chemistry in transition metal selenites.

The transition metal–selenium–oxygen system has been the subject of several previous investigations [2]. Several phases have been reported in which the selenium is found in an oxidation state +IV. This way, transition metal compounds with the $(HSeO_3)^-$, $(SeO_3)^{2-}$ and $(Se_2O_5)^{2-}$ oxoanions are known [3]. Although, a great number of crystal structures related to the selenite compounds have been resolved, studies on the physical properties of the synthesized phases are scarce. The thermal behavior and IR spectroscopy of several phases have been reported [4]. The $M(Se_2O_5)$ compound with a chain structure shows the existence of antiferromagnetic interaction [4]. Mild hydrothermal techniques under autogeneous pressure have allowed the attainment of an astonishing variety of inorganic networks templated by organic species [5]. The preparation of two organically templated zinc and iron(III) open framework selenites has been reported [6]. Recently, we have reported the crystal structure of the $Mn_4(H_2O)(SeO_3)_4$ and $Mn_3(H_2O)(SeO_3)$ [7], synthesized by mild hydrothermal techniques, and the study

* Corresponding author. Tel.: +34 946015523; fax: +34 946013500.
E-mail address: joseluis.mesa@ehu.es (J.L. Mesa).

1386-1425/$ – see front matter © 2007 Elsevier B.V. All rights reserved.
doi:10.1016/j.saa.2007.06.019

of their physical properties. We have also studied the crystal structure and the physical behavior of two polymorphs with the composition $Mn(SeO_3)$, obtained under supercritical conditions [8].

The crystal structures of (**1**) and (**2**) were solved from X-ray single crystal data by Koskenlinna et al. [9] and Giester et al. [10], respectively. The crystal structure of compound (**1**) consists of a three-dimensional framework constructed from (MnO_6) octahedra and $(SeO_3)^{2-}$ selenite groups with trigonal pyramidal geometry. The structure is formed from isolated Mn_2O_{10} edge-sharing octahedral dimers, extended along the [1 0 1] direction. These dimeric entities are connected by the $(SeO_3)^{2-}$ oxoanions (Fig. 1a). The crystal structure of phase (**2**) can be described as a three-dimensional framework composed of (FeO_6) octahedra and $(SeO_3)^{2-}$ selenite anions with trigonal pyramidal geometry. The octahedral entities are linked along the three-crystallographic axes through the selenite oxoanions (Fig. 1b).

In this work, we report the synthesis from aqueous solution and the hydrothermal method of the $Mn(SeO_3)\cdot 2H_2O$ and $Fe_2(SeO_3)_3\cdot 3H_2O$ compounds, respectively. The thermal, luminescent, Mössbauer and magnetic studies are carried out for both phases.

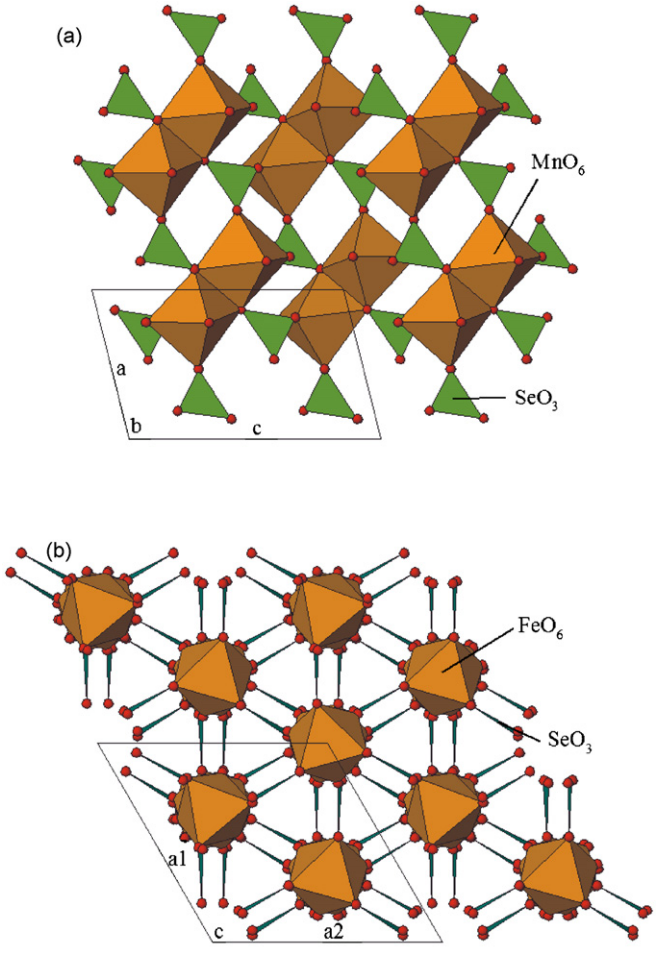

Fig. 1. Polyhedral representation of the three-dimensional crystal structure of (a) compound (**1**) and (b) compound (**2**).

2. Experimental

2.1. Synthesis and characterization

$Mn(SeO_3)\cdot 2H_2O$ has been synthesized in water solution starting from the SeO_2 (9 mmol) and $MnCl_2\cdot 4H_2O$ (5.05 mmol). The pH of the resulting solution was increased up to 1.5 by addition of NH_4OH. Single-crystals with light pink color were obtained by slow evaporation after 20 days, yield 85%. $Fe_2(SeO_3)_3\cdot 3H_2O$ has been obtained by using mild hydrothermal conditions under autogeneous pressure. The starting reagents were SeO_2 (1.44 mmol), $FeCl_3\cdot 6H_2O$ (0.74 mmol), piperazinium (0.075 mmol) and finally HF (0.025 mmol) to decrease the pH down to 1.5. The resulting mixture was dissolved in water and maintained in a politetrafluoroetylene reactor at 110 °C during 5 days. Yellow single-crystals were obtained. Yield 80%.

The single-crystals obtained for both phases were filtered out, washed with water and acetone and dried over P_2O_5 during 6 h. The metal ion and selenium contents were confirmed by inductively coupled plasma atomic emission spectroscopy (ICP-AES) analysis, performed with a RL Fisons 3410 spectrometer. For (**1**), it was found: Se, 35.8; Mn, 24.8. $Mn(SeO_3)\cdot 2H_2O$ requires: Se, 36.2; Mn, 25.2. For (**2**), it was found: Se, 14.5; Fe, 10.0. $Fe_2(SeO_3)_3\cdot 3H_2O$ requires: Se, 14.9; Fe, 10.2. The density of phase (**1**), 3.1(1) g cm^{-3}, was measured by flotation in a mixture of CH_2I_2/CCl_4. In the case of compound (**2**), the density was measured by picnometry using kerosene. The value obtained is 3.4(1) g cm^{-3}.

2.2. X-ray diffraction

X-ray powder diffraction patterns of (**1**) and (**2**), used for the Rietveld analysis, have been recordered with a PHILIPS X'PERT automatic diffractometer (Cu Kα radiation). The spectra were scanned in steps of 0.02° in 2θ for 12 s/step. Rietveld refinements have been performed with the FULLPROF program [11]. Details of the process are given in Table 1. The unit cell parameters obtained after the refinement of both compounds are

Table 1
Details of the Rietveld refinement for $Mn(SeO_3)\cdot 2H_2O$ and $Fe_2(SeO_3)_3\cdot 3H_2O$

Empical formula	$Mn(SeO_3)\cdot 2H_2O$	$Fe_2(SeO_3)_3\cdot 3H_2O$
Formula weight (g/mol)	217.92	546.61
Crystal system	Monoclinic	Trigonal
Space group (Nu.)	$P2_1/n$ (14)	$R3c$ (161)
a (Å)	6.649(1)	9.361(1)
b (Å)	6.542(1)	9.361(1)
c (Å)	10.890(1)	20.276
α (°)	90.0	90
β (°)	103.85(1)	90
γ (°)	90.0	120
Volume (Å^3)	459.9(1)	1538.8(2)
Z	4	6
ρ (calc.)	3.14	3.54
R_{Bragg}, R_f (%)	11.1, 7.82	8.26, 4.38
R_p, R_{wp} (%)	13.6, 18.2	10.9, 14.1
χ^2 (%)	4.52	2.28

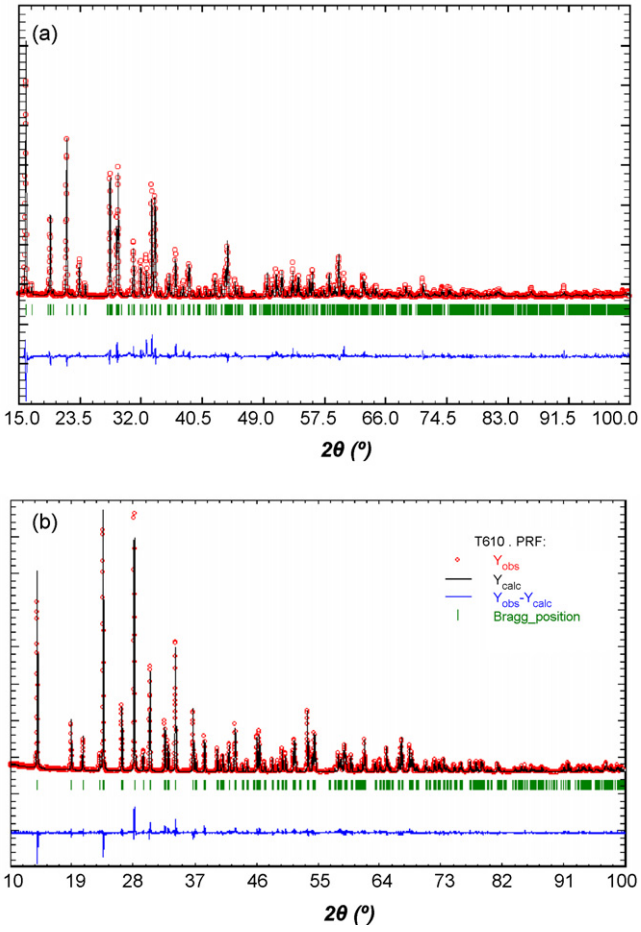

Fig. 2. Observed, calculated and difference X-ray powder diffraction patterns of the (a) compound (**1**) and (b) compound (**2**). The observed data are shown by the dots, the calculated pattern is denoted by the solid line and the difference between the spectra is presented in the lower region.

similar to those described in the literature [$P2_1/c$, $a = 6.655(1)$ Å, $b = 6.542(1)$ Å, $c = 10.900(1)$ Å and $\beta = 103.84(1)°$] for (**1**) [9] and [$R3c$, $a = 9.36(1)$ Å, $c = 20.30(1)$ Å] [10] for (**2**), respectively. The results of the Rietveld refinement are illustrated in Fig. 2.

2.3. Physical measurements

Thermogravimetric measurements were carried out heating the samples at 5 °C min^{-1} under synthetic air in the 30–800 °C temperature range using a SDC 2960 Simultaneous DSC-TA instrument. The IR spectra (KBr pellets) have been obtained with a Nicolet FT-IR 740 spectrophotometer in the 400–4000 cm^{-1} range. The diffuse reflectance spectra were registered at room temperature on a Varian Cary 5000 UV-VIS-NIR spectrometer in the 210–2000 nm range. The excitation and emission luminescent spectra of the manganese compound were recordered with a SPEX Fluorolog 212 spectrofluorometer. Excitation spectrum was corrected for the variation of the incident flux as well as emission spectra for the transmission of the monochromator and the response of the photomultiplier. A Bruker ESP 300 spectrometer was used to record the X-band ESR polycrystalline spectra from room temperature up to 4.2 K. The temperature was stabilized by an Oxford Instrument (ITC 4) regulator. The magnetic field was measured with a Bruker BNM 200 gaussmeter and the frequency inside the cavity was determined using a Hewlett–Packard 5352 microwave frequency counter. Magnetic measurements for powdered sample were performed in the temperature range 5–300 K, using a Quantum Desing MPMS-7 SQUID magnetometer. The magnetic field was 1000 Gauss, a value lying within the range of linear dependence of magnetization versus magnetic field even a 5.0 K.

3. Results and discussion

3.1. Thermal behavior

Compounds (**1**) and (**2**) are stable up to, approximately, 75 and 200 °C, respectively. The elimination of the water molecules (experimental 18.0 and 10.2%, calculated 16.6 and 9.9%, for phases (**1**) and (**2**), respectively) takes place in the 75–300 and 200–350 °C ranges for (**1**) and (**2**), respectively. Above 475 and 460 °C in the case of compounds (**1**) and (**2**), respectively, the decomposition of the $(SeO_3)^{2-}$ anions occurs (experimental 46.5 and 60.5%, calculated 47.2 and 60.9% for (**1**) and (**2**), respectively) giving rise to SeO_2(g). At 700 °C, the inorganic residues are the Mn_2O_3 and Fe_2O_3 oxides for every compound [12].

The thermal behavior of compounds (**1**) and (**2**) was also studied by time resolved X-ray thermodiffractometry. A PHILIPS X'PERT automatic diffractometer (Cu Kα radiation) equipped with a variable temperature stage (Anton Paar HTK16) and a Pt sample holder was used. The data have been recordered in 2θ steps of 0.02° in the range $5 \leq 2\theta \leq 50°$, counting for 1s per step and increasing the temperature at 5 °C min^{-1} from room temperature to 650 °C. The results are reported in Fig. 3. The compounds are stable up to *ca.* 125 and 325 °C, respectively and the intensity of the monitored (0 1 2) peak at, approximately, $2\theta = 22°$ remains practically unchanged. For compound (**1**), a phase, which cannot be identified on the PDF files, appears in the 125–425 °C range. Above 425 °C, the Mn_2O_3 oxide [12] is formed in good agreement with the thermogravimetric data. For phase (**2**), in the 325–475 °C range an amorphous compound is obtained. At higher temperatures a residue of Fe_2O_3 is found [12], in accordance with the thermogravimetric data.

3.2. IR, UV–vis and Mössbauer spectroscopies

In the IR spectra of both phases, the bands belonging to the stretching and deformation modes of the water molecules can be observed at 3450–2590 and 1625, 1545 cm^{-1}, respectively. Three groups of bands have been assigned to the vibrational modes of the $(SeO_3)^{2-}$ oxoanions. The symmetric stretching mode, $\nu_s(SeO_3)^{2-}$ is located at 910 cm^{-1}, the antisymmetric stretching, $\nu_{as}(SeO_3)^{2-}$, splitted at 810, 725 and 590 cm^{-1}, and finally the bending mode, $\delta(SeO_3)^{2-}$ is peaking at 480 cm^{-1} [13].

The diffuse reflectance spectrum of the phase (**1**) shows several weak spin forbidden transitions at 18,410, 22,210, 24,400,

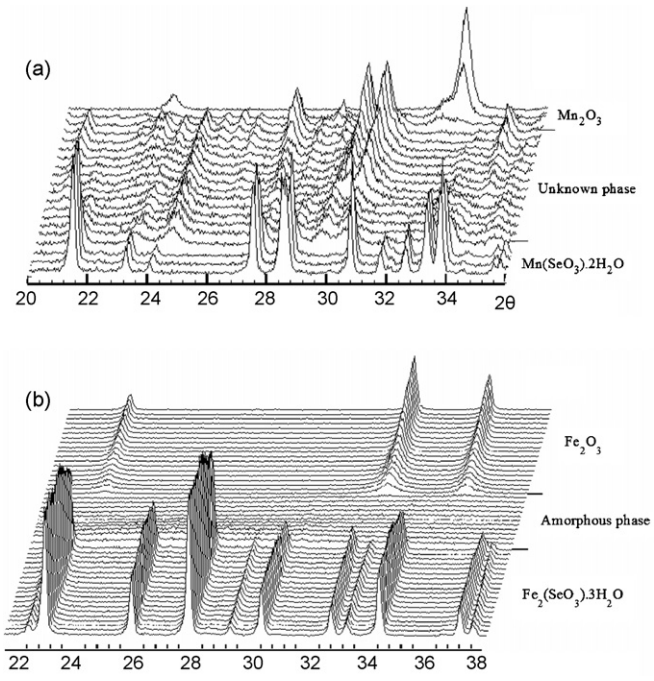

Fig. 3. (a–b) Thermodiffractogram characteristic of the phases (**1**) and (**2**).

28,980 and 31,750 cm^{-1}. The emission spectrum recordered at 6 K presents a band centered at 685 nm (Fig. 4(a)). This result indicates the existence of Mn^{2+} cations in slightly distorted octahedra environments. The excitation spectrum (Fig. 4(b)) shows a spectral distribution of five bands, which correspond to transitions from the $^6A_{1g}(^6S)$ ground state, to the $^4T_{1g}(^4G)$; $^4T_{2g}(^4G)$; $^4A_{1g}(^4G)$, $^4E_g(^4G)$; $^4T_{2g}(^4D)$ and $^4E_g(^4D)$ excited levels at the following frequencies 18,420, 22,220, 24,390, 28,985 and 31,745 cm^{-1}, respectively. The positions of these bands are coherent with those observed on the diffuse reflectance spectrum (continuous line in Fig. 4(b)). The calculated Dq parameter is 790 cm^{-1} and *B* and *C*-Racah parameters are 690 and 3500 cm^{-1}, respectively. The reduction of the *B*-parameter from that of the free Mn^{2+} cation (960 cm^{-1}) is 72%, which indicates a significant covalent character in the Mn–O chemical bonds. All these results are in good agreement with the octahedral coordination of the Mn^{2+}cations [14].

The diffuse reflectance spectrum of the compound (**2**) shows the characteristic features of the Fe^{3+} d^5-high spin cation. The weak forbidden electronic transitions from the $^6A_{1g}(^6S)$ ground state, to the $^4T_{1g}(^4G)$; $^4T_{2g}(^4G)$; $^4A_{1g}(^4G)$, $^4E_g(^4G)$; $^4T_{2g}(^4D)$ and $^4E_g(^4D)$ excited levels are observed at the following frequencies 12,130, 15,615, 20,385, 22,225 and 29,575 cm^{-1}, respectively. The calculated Dq parameter is 1015 cm^{-1} and *B*- and *C*-Racah parameters are 615 and 2850 cm^{-1}, respectively. The reduction of the *B*-parameter from that of the free Fe^{3+} cation (1150 cm^{-1}) is 55%, which indicates a significant covalent character in the Fe–O chemical bonds. These results are in good agreement with the existence of octahedrically coordinated Fe^{3+} cations [14] and confirm the structural results.

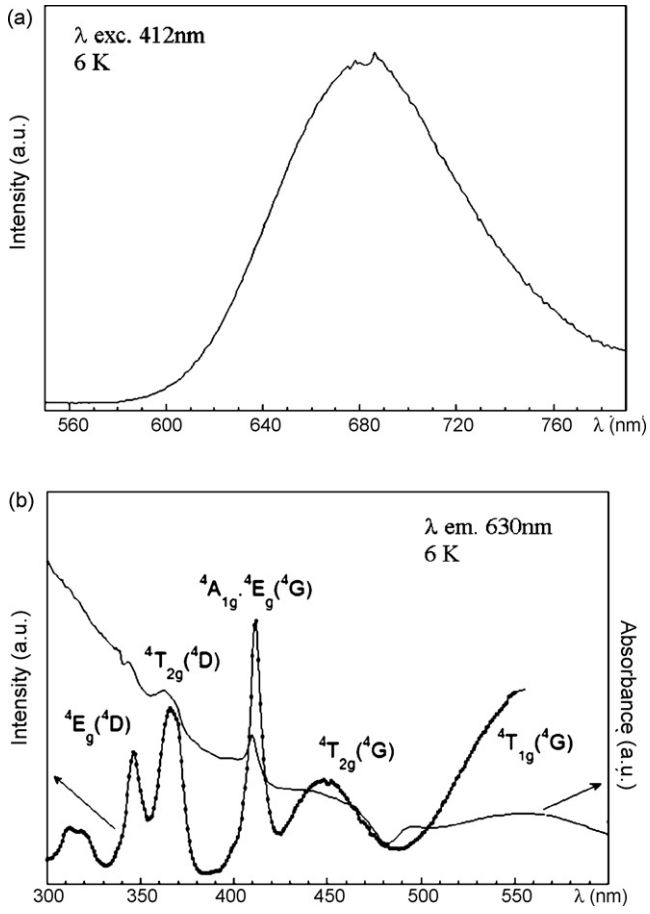

Fig. 4. (a) Luminescent emission spectrum (λ excitation 412 nm) at 6 K (b) Luminescent excitation spectrum (λ emission 630 nm) at 6 K for (**1**).

The Mössbauer spectrum of (**2**) in the paramagnetic state at 300 K shows two singlets corresponding to the pure electrostatic interactions of the two crystallographic independent Fe^{3+} cations, located in a very regular octahedral environment (Fig. 5). The values of the isomer shift obtained from the fit of the spectrum by using the NORMOS program [15] are 0.36(2) and 0.46(2) mm s^{-1} for Fe(1) and Fe(2) sites, respectively.

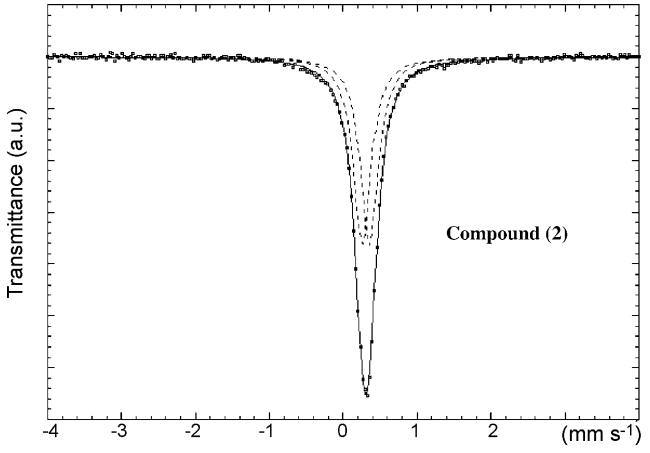

Fig. 5. Mössbauer spectrum at 300 K of the compound (**2**).

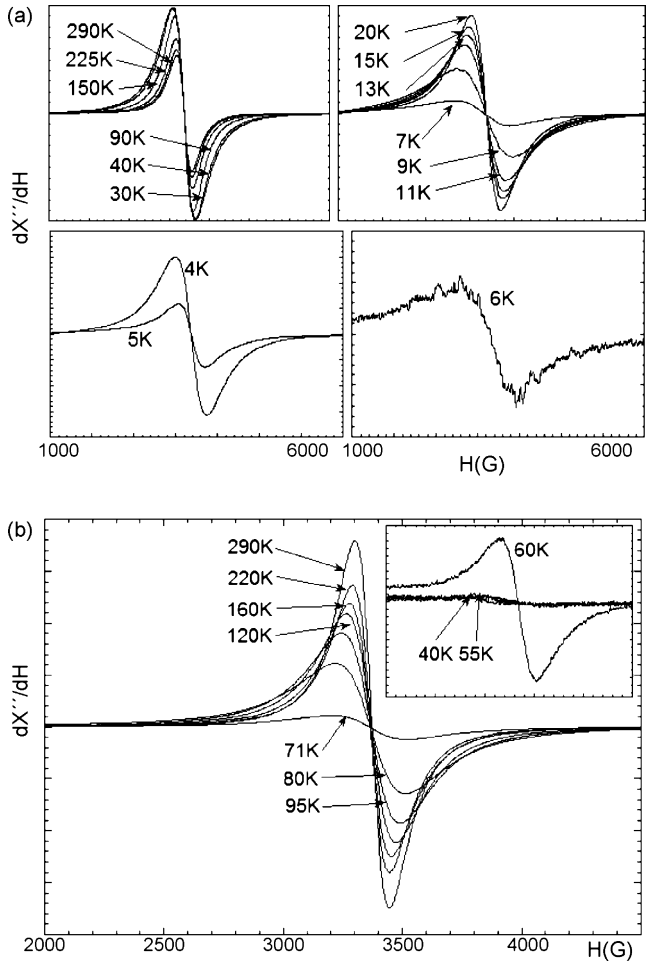

Fig. 6. Powder X-band ESR spectra of (a) compound (**1**) and (b) compound (**2**).

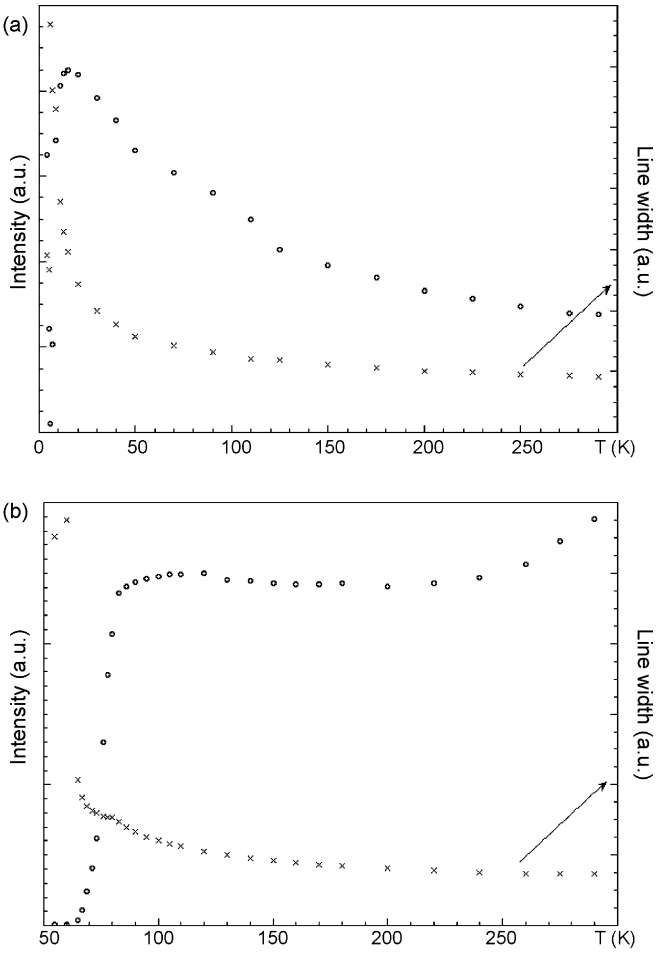

Fig. 7. Temperature dependence of the intensity and the line-width of the ESR signals for (a) compound (**1**) and (b) compound (**2**).

3.3. ESR and magnetic properties

The ESR spectra of compounds (**1**) and (**2**) remain isotropic from 4.2 K to room temperature for (**1**) and from 40 K to room temperature for (**2**) (Fig. 6). At approximately 40 K the signal disappears in (**2**) probably due to a spin change in the iron cations (5/2 to 2). The ESR signals of both phases were fitted to Lorentzian curves and then calculated the value of the *g*-gyromagnetic tensor, 1.99(1) and 2.00(1), respectively, in good agreement with the existence of Mn(II) and Fe(III) d^5-cations, respectively.

For (**1**), the thermal evolution of the intensity of the signals increases with decreasing temperature and shows a maximum at approximately 25 K. This result suggests the existence of antiferromagnetic interactions. After this temperature the intensity decreases down to 4.2 K (Fig. 7(a)). The thermal variation of the line-width of the ESR signals increases slowly up to 50 K and below this temperature the line-width increases dramatically due to a phenomenon of spin correlation [16].

For phase (**2**), the thermal evolution of the intensity of the signals decreases slightly with decreasing temperature down to, approximately, 240 K (Fig. 7(b)). Below this temperature the intensity remains constant and then decreases dramatically down to, approximately, 40 K. This effect could be associated to a change in the spin of the iron atoms, from 5/2 to 2. Finally, the ESR signal disappears below 40 K. These results are in good agreement with the existence of antiferromagnetic interactions. The line-width of the signals shows a slow increase with decreasing temperature up to 80 K. Below this temperature it increases dramatically up to 40 K due to a phenomenon of spin correlation [16].

The molar magnetic susceptibility, χ_m, of the compound (**1**) exhibits a sharp maximum at approximately 8 K, indicating that a three-dimensional magnetic ordering is established around this temperature, taking into account the structural features of this phase (Fig. 8(a)). The compound follows a Curie–Weiss law in the 15–300 K range, with values of the Curie and Curie–Weiss constants of $C_m = 4.38\ cm^3$ K/mol and $\theta = -15.1$ K. The $\chi_m T$ versus T curve decreases at room temperature from 4.17 cm^3 K/mol down to 0.70 cm^3 K/mol at 5 K. Both results, the negative Weiss temperature and the continuous decreasing of the $\chi_m T$ versus T curve confirm the antiferromagnetic interactions in the $Mn(SeO_3)\cdot 2H_2O$ compound. The "*J*"-exchange parameter has been calculated by fitting the experimental magnetic data to a 3D antiferromag-

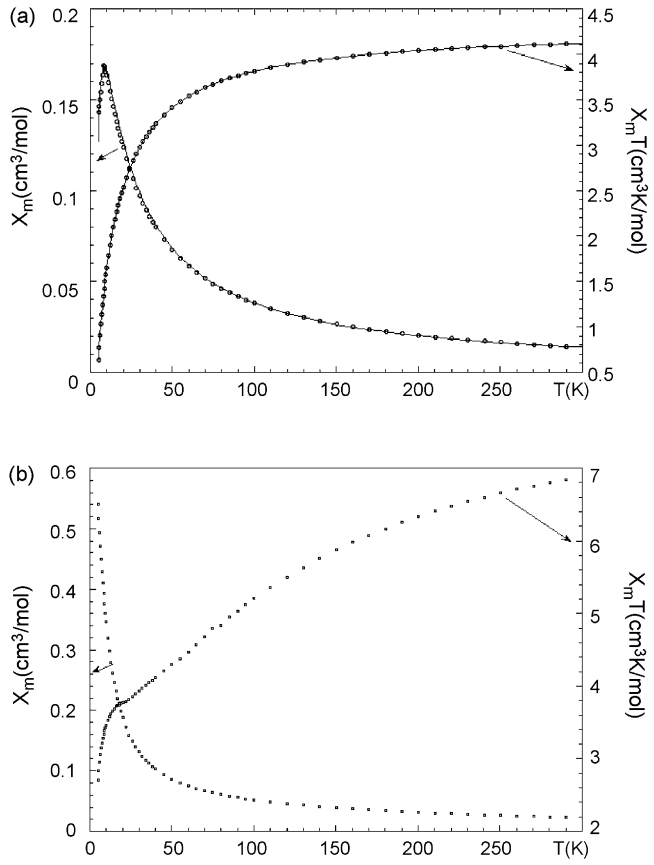

Fig. 8. Thermal variation of the χ_m and $\chi_m T$ vs. T curves for (a) compound (**1**) and (b) compound (**2**).

netic cubic lattice by using the Rushbrooke and Wood equation (1) [17]:

$$\chi_m = \frac{(35Ng^2\beta^2)/(12KT)}{1 + (35/x) + (221.67/x^2) + (608.22/x^3) + (26049.6/x^4) + (210986.5/x^5) + (8,014,980/x^6} \quad (1)$$

where $x = (KT/J)$, N is the Avogadros's number, β the Bohr's magneton and K is the Boltzmann's constant. The results of the fit are given by the solid line in Fig. 8(a). The value obtained for the J/K exchange parameter is -0.35 K.

The molar magnetic susceptibility, χ_m, of phase (**2**) increases continuously from room temperature to 5.0 K (Fig. 8(b)). The compound follows the Curie–Weiss law in the 100–300 K range, with values of the Curie and Curie–Weiss constants of $C_m = 8.27$ cm^3 K/mol and $\theta = -60.7$ K. The $\chi_m T$ versus T curve decreases continuously from 6.89 cm^3 K/mol at room temperature down to 3.8 cm^3 K/mol at 20 K (see Fig. 8(b)). Below this temperature, the curve decreases dramatically down to 2.70 cm^3 K/mol at 5.0 K. Similarly to that found in the thermal evolution of the intensity of the ESR-signals, this result is probably due to a change in the spin of the iron cations, from 5/2 to 2. Both, the negative Weiss temperature and the continuous decreasing of the $\chi_m T$ versus T curve confirm the antiferromagnetic interactions in the $Fe_2(SeO_3)_3{\cdot}3H_2O$ compound.

4. Concluding remarks

Compounds (**1**) and (**2**) were obtained from different synthetic methods. The $Mn(SeO_3){\cdot}2H_2O$ phase was synthesized by slow evaporation from a saturated aqueous solution. The $Fe_2(SeO_3)_3{\cdot}3H_2O$ compound was obtained using mild hydrothermal conditions under autogeneous pressure in water solution. The crystal structure of both phases was refined using the Rietveld method. Both structures are three-dimensional. The framework of (**1**) is constructed from MnO_6 octahedra and $(SeO_3)^{2-}$ trigonal pyramids. The crystal structure of (**2**) is formed by two FeO_6 crystallographically independent octahedra and $(SeO_3)^{2-}$ groups with trigonal pyramidal geometry. The IR spectra of both phases show the characteristic bands of the selenite oxoanion. The compounds are stable up to 75 and 200 °C, respectively, after these temperatures the elimination of the water molecules occurs and the decomposition of the selenite oxoanions giving rise to SeO_2(g). The luminescent measurements in (**1**) are in good agreement with the existence of Mn^{2+} cations in a slightly distorted octahedral environment. The diffuse reflectance spectrum and the Mössbauer measurements performed in the paramagnetic state of (**2**), are consistent with the existence of Fe^{3+} d^5-cations in slightly distorted octahedral geometry. ESR spectra of both compounds are isotropic and the thermal evolution of the intensity of the signals suggests an antiferromagnetic behavior, which has been confirmed by the magnetic measurements. For phase (**1**) the J-exchange parameter has been calculated, obtaining a value of -0.35 K. For (**2**) the thermal evolution of the ESR signals and the magnetic susceptibility suggest a change of spin from Fe^{3+} ($S = 5/2$) to Fe^{2+} ($S = 2$) at low temperatures.

Acknowledgements

This work has been financially supported by the "Ministerio de Educación y Ciencia" (MAT-2004-02071) and the "Universidad del País Vasco" (UPV/EHU) (9/UPV00130.310-15967/2004; 9/UPV00169.310-13494/2001). The authors thank the technician of SGIker, Dr. I. Orue, financed by the "National Program for the Promotion of Human Resources within the National Plan of Scientific Research, Development and Innovation "Ministerio de Ciencia y Tecnología" and "Fondo Social Europeo (FSE)", for magnetic measurements. Dr. A. Larrañaga wishes to thank the Gobierno Vasco/Eusko Jaurlaritza for funding.

References

[1] S.M. Kauzlarich, J.M. Dorhout, J. Honig, J. Solid State Chem. 149 (2000) 3.

[2] M. Koskenlinna, in: J. Koskikallio (Ed.), Structural Features of Selenium(IV) Oxoanions Compounds, Helsinki University of Technology, 1996.
[3] (a) B. Engelen, K. Boldt, K. Unterderweide, U. Baumer, Z. Anorg. Allg. Chem. 621 (1995) 331;
(b) M. Koskelinna, J. Kansikas, T. Leskela, Acta Chem. Scand. 48 (1994) 783;
(c) Z. Micka, I. Nemec, P. Vojtiseck, J. Ondraced, J. Holsa, J. Solid State Chem. 112 (1994) 237;
(d) J. Valkonen, M. Koskelinna, Acta Chem. Scand. Ser. A 32 (1978) 603;
(e) W.T.A. Harrison, G.D. Stucky, A.K. Cheetham, Eur. J. Solid State Inorg. Chem. 30 (1999) 347;
(e) M. Wildner, Monastch. Chem. 122 (1991) 585;
(f) A.V.P. MacManus, W.T.A. Harrison, A.K. Cheetham, J. Solid State Chem. 92 (1991) 253;
(g) H. Effenberger, J. Solid State Chem. 70 (1987) 303;
(h) W.T.A. Harrison, G.D. Stucky, R.E. Morris, A.K. Cheetham, Acta Crystallogr., Sect. C 48 (1992) 1365;
(i) M. Koskelinna, L. Niinisto, J. Valkonen, Acta Chem. Scand., Ser. A 30 (1976) 836;
(j) G. Meunier, M. Bertaud, Acta Crystallogr., Sect. B 30 (1974) 2840;
(k) F.C. Hawthorne, L.A. Groat, T.S. Ercit, Acta Crystallogr., Sect. C 43 (1987) 2042;
(l) W.T.A. Harrison, A.V.P. McManus, A.K. Cheetham, Acta Crystallogr., Sect. C 48 (1992) 412.
[4] (a) H. Muilu, J. Valkonen, Acta Chem. Scand. Ser. A 41 (1987) 183;
(b) Z. Micka, I. Nemec, P. Vojtisek, J. Ondracek, J. Holsa, J. Solid State Chem. 112 (1994) 237;
(c) J. Bovoisin, J. Galy, J.C. Tombe, J. Solid State Chem. 170 (1993) 171.
[5] A.K. Cheetham, G. Ferey, T. Liosseau, Angew. Chem., Int. Ed. 38 (1999) 3268.
[6] (a) W.T.A. Harrison, M.K.L. Phillips, J. Stanchfield, T.N. Nenoff, Angew. Chem., Int. Ed. 39 (2000) 3808;
(b) A. Choudhury, U. Kumar, C.N.R. Rao, Angew. Chem., Int. Ed. 41 (2002) 158.
[7] A. Larrañaga, J.L. Mesa, J.L. Pizarro, R. Olazcuaga, M.I. Arriortua, T. Rojo, J. Chem. Soc., Dalton Trans. (2002) 3447.
[8] A. Larrañaga, J.L. Mesa, J.L. Pizarro, L. Lezama, J.P. Chapman, M.I. Arriortua, T. Rojo, Dalton Trans. (2005) 1727.
[9] M. Koskenlinna, J. Niiniströ, J. Valkonen, Cryst. Struct. Commun. 5 (1976) 663.
[10] G. Giester, F. Pertlik, J. Alloys Compd. 210 (1994) 125.
[11] J. Rodríguez Carvajal, FULLPROF, Rietveld Pattern Matching Analysis of Powder Patterns, unpublished results, 1994.
[12] Powder Diffraction File—Inorganic and Organic, ICDD, Pennsylvania, USA, 1995 (numbers 78-390 and 87-1166).
[13] K. Nakamoto, Infrared and Raman Spectra of Inorganic and Coordination Compounds, John-Wiley & Sons, New York, 1997.
[14] A.B.P. Lever, Inorganic Electronic Spectroscopy, Elsevier Science Publishers B.V., Amsterdam, the Netherlands, 1984.
[15] R.A. Brand, J. Larner, D.M. Herlach, J. Phys. F14 (1984) 555.
[16] (a) H.W. Wijn, L.R. Walker, J.L. Daris, H. Guggenheim, J. Solid State Chem. 11 (1972) 803;
(b) P.M. Richards, M.B. Salamon, Phys. Rev. B 9 (1974) 32;
(c) A. Bencini, D. Gatteschi, EPR of Exchange Coupled Systems, Springer-Verlag, Berlin, 1990;
(d) T.T.P. Cheung, Z.G. Soos, R.E. Dietz, F.R. Merrit, Phys. Rev. B 17 (1978) 1266.
[17] G.S. Rushbrooke, P.S. Wood, Mol. Phys. 1 (1958) 257.